Advances in Water Resources 34 (2011) 1335–1342

Contents lists available at ScienceDirect

Advances in Water Resources

journal homepage: www.elsevier.com/locate/advwatres

Assessment of critical path analyses of the relationship between permeability and electrical conductivity of pore networks

Todd H. Skaggs *

US Salinity Laboratory, USDA-ARS, Riverside, CA, United States

ARTICLE INFO

Article history:
Received 8 February 2011
Received in revised form 22 June 2011
Accepted 26 June 2011
Available online 13 July 2011

Keywords:
Critical path analysis
Pore network model

ABSTRACT

Critical path analysis (CPA) is a method for estimating macroscopic transport coefficients of heterogeneous materials that are highly disordered at the micro-scale. Developed originally to model conduction in semiconductors, numerous researchers have noted that CPA might also have relevance to flow and transport processes in porous media. However, the results of several numerical investigations of critical path analysis on pore network models raise questions about the applicability of CPA to porous media. Among other things, these studies found that (i) in well-connected 3D networks, CPA predictions were inaccurate and became worse when heterogeneity was increased; and (ii) CPA could not fully explain the transport properties of 2D networks. To better understand the applicability of CPA to porous media, we made numerical computations of permeability and electrical conductivity on 2D and 3D networks with differing pore-size distributions and geometries. A new CPA model for the relationship between the permeability and electrical conductivity was found to be in good agreement with numerical data, and to be a significant improvement over a classical CPA model. In sufficiently disordered 3D networks, the new CPA prediction was within ±20% of the true value, and was nearly optimal in terms of minimizing the squared prediction errors across differing network configurations. The agreement of CPA predictions with 2D network computations was similarly good, although 2D networks are in general not well-suited for evaluating CPA. Numerical transport coefficients derived for regular 3D networks of slit-shaped pores were found to be in better agreement with experimental data from rock samples than were coefficients derived for networks of cylindrical pores.

Published by Elsevier Ltd.

1. Introduction

A fundamental problem of subsurface hydrology is the interpretation and prediction of macroscopic properties of porous media based on the microscopic structure of pores [1,13,16,42]. In the last few decades, many researchers have employed percolation theory in the quest for a micro-scale understanding of porous media; reviews may be found, for example, in Berkowitz and Balberg [6], Berkowitz and Ewing [7], and Hunt and Ewing [21]. The focus of this paper is a methodology known as critical path analysis (CPA), a technique that uses elements of percolation theory to calculate macroscopic transport coefficients of heterogeneous materials [3,20,21].

The basic idea of CPA is that in a strongly heterogeneous medium, most transport occurs along a relatively small number of high conductance pathways. Transport along these high conductance pathways is constrained by their least conductive sections, which act as "bottlenecks" to transport. Thus the size and frequency of the bottlenecks determine to a large degree the overall macroscopic transport properties.

CPA relies on percolation theory to enumerate the various quantities needed to derive macroscopic transport coefficients, such as path separation distance and frequency of bottlenecks. For example, a characteristic value for the bottleneck conductance can be determined by considering a related percolation problem. Specifically, in a heterogeneous medium with a variable local conductance g, the characteristic or critical conductance value, g_c, is defined to be the largest conductance such that the set of conductances $g > g_c$ forms a spanning cluster. This may be expressed as [3]

$$p_c = \int_{g_c}^{\infty} f_g(g)dg \tag{1}$$

where $f_g(g)$ is the probability density function for the local or micro-scale conductance g, and p_c is the percolation threshold for the system.

CPA was originally developed to analyze conduction in disordered systems such as amorphous semiconductors [3,12]. In these systems, the local conductances are exponential functions of random system parameters which are uniformly distributed, and thus the local conductances follow a log-uniform distribution such that

* Address: US Salinity Laboratory, 450 W. Big Springs Rd., Riverside, CA 92507, United States. Tel.: +1 951 369 4853; fax: +1 951 342 4964.
E-mail address: Todd.Skaggs@ars.usda.gov

0309-1708/$ - see front matter Published by Elsevier Ltd.
doi:10.1016/j.advwatres.2011.06.010

Nomenclature

CPA	acronym for critical path analysis
CV	coefficient of variation
EC_b	bulk electrical conductivity
EC_w	electrical conductivity of saturating fluid
b	breadth of slit-shaped pore
g_0	proportionality constant in the pore conductance model
d	spatial dimension (equals 2 or 3)
f_g	pore conductance probability density function
f_δ	pore-size probability density function
g	pore conductance
g_c	critical pore conductance
k	fluid permeability
k^*	normalization constant
K	hydraulic conductivity
l_0	pore length
m	exponent in pore conductance model
p_c	percolation threshold
W	parameter in log-uniform conductance model
y	CPA conductivity prefactor exponent
α	parameter in power law pore-size distribution
β	parameter in power law conductance distribution
δ	characteristic length of pore cross section (termed "pore-size")
δ_c	critical pore-size
$\delta_{\min}$	lower bound for δ
$\delta_{\max}$	upper bound for δ
δ_g	geometric mean pore-size
η	fluid viscosity
λ	conductivity length scale
μ	mean of $\ln\delta$
ν	percolation correlation length exponent
σ	standard deviation of $\ln\delta$

$$f_g(g) = \frac{1}{Wg} \tag{2}$$

where $W \gg 1$ is a parameter specifying the broadness of the distribution and hence the degree of heterogeneity or disorder in the system. For sufficiently large W, CPA leads to an estimation of the macroscopic conductivity, Σ, that is given by [19]

$$\Sigma = CW^{-y}g_c \tag{3}$$

where C is a system dependent constant and y is termed the prefactor exponent. Numerical calculations of the conductivity of 3D networks are in general agreement with the form of Eq. (3) [38,39].

The form of Eq. (3) implies that the average separation between high conductance pathways is a distance λ that goes like $\lambda \sim W^y$ [39]. Thus the distance between pathways increases with increasing heterogeneity (increasing W). The prefactor exponent y is presumed to be a universal exponent such that its value depends only on the spatial dimension of the system. One hypothesis [31] is that the exponent is given by $y = (d-2)\nu$, where d is the spatial dimension and ν is the correlation length exponent from percolation theory (the latter known to be $\nu = 0.88$ for $d = 3$ and $\nu = 4/3$ for $d = 2$ [41]). With that formulation, $y = 0.88$ for 3D systems and $y = 0$ for 2D systems. Numerical simulations are generally in agreement with $y = 0$ for 2D systems, but have found that $y < 0.88$ for 3D systems [28,30,39,43]. For example, Skaggs [39] estimated $y \approx 0.74$ based on simulations of a 3D system with the local conductances following the log-uniform distribution specified by Eq. (2).

Hunt [20,21] has noted that differences may exist between the nature of the disorder found in semiconductors (e.g. Eq. (2)) and that typically found in porous media, such that the success of CPA in semiconductor physics does not necessarily imply that CPA is applicable to either fluid flow or electrical conduction in porous media. Nevertheless, the literature contains several apparently successful applications to porous media. Perhaps the best known result was that obtained by Katz and Thompson [26,27]. In porous media, the critical conductance can be expressed in terms of a critical characteristic pore diameter, δ_c. Using such a relationship, Katz and Thompson [26] derived the following result for saturated porous media,

$$\frac{k}{EC_b/EC_w} = c_{KT}\delta_c^2 \tag{4}$$

where k is the fluid permeability, δ_c is the critical pore diameter, EC_b is the bulk electrical conductivity, EC_w is the electrical conductivity of the saturating fluid, and $c_{KT} \approx 1/226$ is a numerical constant. Eq. (4) has no free parameters if δ_c can be measured. Katz and Thompson [26,27] determined δ_c on rock samples using mercury intrusion measurements. Very good agreement was obtained between Eq. (4) and measurements made on a variety of rock samples.

More recently, Hunt et al. [20–24] have applied critical path analysis using continuum percolation and a fractal pore distribution model to derive expressions for the hydraulic conductivity and water retention functions of unsaturated soils. In these models, the critical length scale (pore size) is related to the bubbling pressure. Hunt and Gee [22–24] had success comparing their models against various experimental data. In these studies, bubbling pressures and critical volume fractions were not measured directly; instead, an empirical result from a diffusion study by Moldrup et al. [35] was adopted to estimate these quantities.

As noted by David [15] and Bernabé [8], the experimental results of Agrawal et al. [2] can also be considered consistent with the CPA conception of transport processes. In that work [2], molten Wood's metal was injected into rock samples of known permeability and then "frozen", thereby effectively removing the pores penetrated by the metal from the active pore space. Agrawal et al. [2] observed that permeability was reduced by as much as a factor of 4 when the saturation of the Wood's metal was only about 10% and presumably confined to only the "critical" percolating path. Thus the critical pathway accounted for about 75% of the original rock permeability. Additional experimental evidence is provided by Lukasiewicz and Reed [34], who found that the permeability of porous alumina compacts with porosities ranging from 32 to 50% was controlled by a mean radius length that was related to Katz and Thompson's critical radius [37].

On the other hand, several numerical tests of CPA on network models of porous media have produced mixed results which raise some questions about the interpretation of the experimental results. Bernabé [8] found that macroscopic properties of 2D networks were strongly related to δ_c, but cautioned that CPA was probably not valid for the simulated conditions and did not likely provide the explanation for the significance of δ_c. Among the reasons for this caution was the observation that only about 20% of the flow occurred on the critical path in networks that where highly connected (high coordination number).

Bernabé and Bruderer [9] investigated the effect of the variance of the pore-size distribution on 2D network transport properties. For various pore-size distribution models, they found that when pore-size variance (heterogeneity) was large, certain network transport coefficients were proportional to the square of the

critical radius, as predicted by Katz and Thompson [26]. Again, however, these authors noted that the observed flow pathways, although "localized", were not restricted to the "critical path", and concluded that "the predominant role played by the critical [pore diameter] cannot be explained by CPA" [9].

Friedman and Seaton [18] performed 3D network simulations investigating the effects of pore-size distribution and lattice coordination number. These authors found "reasonable" agreement between the data and CPA predictions, noting that the agreement was good whenever network connectivity (coordination number) was low, but that the agreement became significantly worse when connectivity increased. Also, an examination of the data presented in Fig. 5 of Friedman and Seaton [18] indicates that the relative prediction error increased (seemingly towards an asymptotic value) when the broadness of the pore-size distribution increased, an unexpected result given that CPA is normally expected to be most applicable when there is strong disorder, i.e. a broad pore-size distribution.

Taken collectively, these simulation studies raise some questions about the applicability of CPA to porous media and the proper interpretation of the experimental results noted above. To what degree is the CPA conceptualization of localized transport realized in porous media? Is the apparent significance of δ_c due to the argument made by CPA, or is it instead because of the coincidental correlation of δ_c with other significant length scales? Resolving these questions about the CPA approach is important because if CPA lacks a strong physical basis there is little practical advantage to be gained over conventional empirical constitutive models.

The objective of the present work was to clarify the performance of CPA when applied to network models of porous media.

2. Theory and methods

2.1. Pore network model

Consider a network of liquid-saturated pores arranged on a regular lattice with fixed pore length l_0. The conductance, g, of a pore is given by

$$g = g_0 \delta^m \tag{5}$$

where δ is a characteristic length of the pore cross-section and g_0 and m are constants that depend on pore geometry and on the nature of the transport, i.e. viscous flow or electrical current. Thus g may refer to either hydraulic or electrical conductance. Examples of the length δ are the pore diameter in the case of cylindrical pores and the pore width in the case of slit-shaped pores. For convenience I will refer to δ as the "pore-size" when the discussion is not specific to a particular geometry. As is standard in critical path analyses, g is assumed to be uncorrelated in space. This assumption may not be overly restrictive even though many porous media exhibit at least short range spatial correlations in pore properties; Liang et al. [33], working with 3D stochastic pore models derived from image analysis, found that after taking into account changes in the percolation threshold brought about by correlation, Eq. (4), which has the same form as the results derived herein, was "remarkably" accurate when applied to porous media with spatially correlated pore conductances. See Hunt and Idriss [25] for further discussion of percolation-based treatments of the conductivity of spatially correlated media.

Following Friedman and Seaton [18], I consider two particular examples for the pore geometry: cylindrical pores and slit-shaped pores, the latter having a width δ that is much narrower than its breadth b (b is constant in the network). Letting η be the dynamic fluid viscosity and $\pi = 3.14\ldots$, the constants in Eq. (5) for these two geometries are [5,18]:

Cylindrical pores

$$m = 2, \quad g_0 = \pi E C_w/(4 l_0) \quad \text{(electrical conductance)} \tag{6}$$

$$m = 4, \quad g_0 = \pi/(128 \eta l_0) \quad \text{(hydraulic conductance)} \tag{7}$$

Slit-shaped pores

$$m = 1, \quad g_0 = E C_w b/l_0 \quad \text{(electrical conductance)} \tag{8}$$

$$m = 3, \quad g_0 = b/(12 \eta l_0) \quad \text{(hydraulic conductance)} \tag{9}$$

2.2. Pore-size and conductance distributions

Two probability density functions for the pore-size δ are considered.

2.2.1. Power law distribution

Several past investigations of porous media have found that the pore-size density function, f_δ, can be modeled as a truncated power law distribution [4,17,21]. A generic model of this type is given by

$$f_\delta(\delta) = A_\delta \delta^{-\alpha-1} \tag{10}$$

where $\delta_{\min} \leqslant \delta \leqslant \delta_{\max}$, α is the distribution shape parameter, and $A_\delta = \alpha/(\delta_{\min}^{-\alpha} - \delta_{\max}^{-\alpha})$ is the normalization constant ($\alpha \neq 0$). The pore conductance distribution for such a porous medium can be derived from Eqs. (5) and (10):

$$f_g(g) = A_g g^{-\beta-1} \tag{11}$$

where $\beta = \alpha/m$ and $A_g = A_\delta/(m g_0^{-\beta})$. For $\beta \to 0$, this conductance distribution approaches $f_g \sim g^{-1}$, the logarithmically broad conductance distribution for which CPA was originally developed (cf. Eq. (2)).

2.2.2. Lognormal distribution

Another commonly used pore-size density function is the lognormal distribution [18,29]. Letting μ and σ be, respectively, the mean and standard deviation of $\ln\delta$, the lognormal distribution is

$$f_\delta(\delta) = \frac{1}{\sqrt{2\pi}\sigma\delta} \exp\left[-\left(\frac{\ln\delta - \mu}{\sqrt{2}\sigma}\right)^2\right] \tag{12}$$

which may be abbreviated $\mathrm{LN}(\mu,\sigma)$. From Eqs. (5) and (12), the corresponding conductance distribution is

$$f_g(g) = \mathrm{LN}(m\mu + \ln g_0, m\sigma) \tag{13}$$

2.3. Critical path analysis

2.3.1. Generalized conductivity

Different versions of CPA exist. All versions consider that transport is restricted by bottleneck conductances with some characteristic or critical value, but different conductivity calculations are possible depending on assumptions made about the frequency of the bottlenecks and how their separation varies with the degree of system heterogeneity. I use a formulation proposed by Tyč and Halperin [19,43] that is a generalization of Eq. (3),

$$\Sigma = C g_c [g_c f_g(g_c)]^y \tag{14}$$

In the context of the present work, Σ is a generic conductivity that may represent either the hydraulic conductivity, K, or the bulk electrical conductivity, EC_b. Eq. (14) is an estimation that is expected to be applicable when f_g is broad, which Tyč and Halperin [19,43] suggest occurs when $g_c f_g(g_c) \ll 1$ and $g f_g(g)$ is slowly varying in a large neighborhood about g_c. The latter condition is satisfied, for example, if in the vicinity of $g = g_c$, $f_g(g)$ is roughly $f_g(g) \sim g^{-1}$, such that $g f_g(g)$ is approximately constant in that neighborhood (cf. Eq. (2)).

Substitution of a model pore conductance distribution (Eq. (11) or (13)) into Eq. (14) leads to an expression for the generalized

conductivity in terms of pore conductances. Subsequently, Eq. (5) can be substituted to obtain an expression for the generalized conductivity in terms of pore sizes. The following results are obtained for the two model distributions:

Power law distribution

$$\Sigma = Cg_0 A_\delta^y m^{-y} \delta_c^{m-\alpha y} \tag{15}$$

Lognormal distribution

$$\Sigma = Cg_0 (2\pi)^{-y/2} (\sigma m)^{-y} \delta_c^m \exp\left[-y\left(\frac{\ln \delta_c - \mu}{\sqrt{2}\sigma}\right)^2\right] \tag{16}$$

2.3.2. Hydraulic and electrical properties

The relationship between hydraulic and electrical properties is of both theoretical and practical interest (e.g. [36,40,44]). In the current work, formulating the ratio of the hydraulic and electrical conductivities of the same pore network also has the practical advantage of eliminating many system dependent constants. Taking m_H, m_E, $g_{0;H}$, and $g_{0;E}$ to be particular values of the constants in Eq. (5), the following expression is obtained for both the power law (Eq. (15)) and lognormal (Eq. (16)) distributions:

$$\frac{K}{EC_b} = \frac{\Sigma(m_H, g_{0;H})}{\Sigma(m_E, g_{0;E})} = \frac{g_{0;H}}{g_{0;E}} \left(\frac{m_H}{m_E}\right)^{-y} \delta_c^{m_H - m_E} \tag{17}$$

Thus applying the CPA model for the ratio of the hydraulic and electrical conductivities (Eq. (17)) does not require detailed knowledge of the underlying pore distribution, only the value of the critical pore size. On the other hand, the pore geometry is potentially significant. Defining $k \equiv K \times \eta$ to be the fluid permeability, δ_g to be the geometric mean pore-size, EC_w to be the electrical conductivity of the saturating fluid, and k^* to be a pore geometry-dependent scaling factor, Eq. (17) may be expressed in non-dimensional form as:

Cylindrical pores

$$\frac{k/k^*}{EC_b/EC_w} = 2^{-y}(\delta_c/\delta_g)^2, \quad k^* \equiv \delta_g^2/32 \tag{18}$$

Slit-shaped pores

$$\frac{k/k^*}{EC_b/EC_w} = 3^{-y}(\delta_c/\delta_g)^2, \quad k^* \equiv \delta_g^2/12 \tag{19}$$

Eqs. (18) and (19) may be compared with an expression obtained by Friedman and Seaton [18] using an alternative classical CPA model. According to the classical model, k/EC_b is found by considering the ratio of the critical hydraulic and electrical conductances. Using the notation and conventions of the present paper, their result may be written as

$$\frac{k/k^*}{EC_b/EC_w} = (\delta_c/\delta_g)^2 \tag{20}$$

with k^* defined as in Eqs. (18) and (19) for cylindrical and slit-shaped pores, respectively.

The CPA conductivity exponent y is presumed to be universal, such that its value depends only on the dimension of the system. For 2D systems, the exponent is generally accepted to be $y \approx 0$. In this case, no difference exists between the classical result (Eq. (20)) and that obtained in this work (Eqs. (18) and (19)). For 3D systems, however, estimates for y are in the range 0.6–0.88 [39], and thus the new predictions differ from the classical result by a numerical factor of 2^{-y} in the case of cylindrical pores and 3^{-y} in the case of slit-shaped pores. In this work, 3D CPA predictions are made with $y = 0.74$, the value estimated by Skaggs [39] based on analyses of systems with a log-uniform conductance distribution (Eq. (2)).

2.4. Monte Carlo simulations

To assess the accuracy of the CPA models presented in the previous section, numerical simulations were performed to determine the actual permeability and electrical conductivity of various pore network models. For each simulation, a network with uncorrelated random pore-sizes (δ) was generated according to one of the two probability density models considered above (Eqs. (10) and (12)). Individual pore conductances were then set based on Eq. (5), with the parameter values for g_0 and m being determined by the pore geometry used in the network and whether the computation was for electrical or hydraulic conductivity (Eqs. (6)–(9)). A fixed potential was maintained on two opposite sides of the network such that a unit potential drop existed across the network. On the remaining faces, no-flow boundary conditions were maintained. Enforcing mass (or charge) conservation at each node leads to a system of equations that was solved for the nodal potentials using the conjugate gradient method with a block incomplete factorization [39]. The conductivity was then determined based on the computed flow in the network. Computations for the permeability and electrical conductivity were done for each network realization and their ratio calculated. One hundred realizations of each network configuration were generated, and the arithmetic mean result for each configuration is reported below, which was not significantly different from the geometric mean, harmonic mean, and median values.

Three lattices were used for the pore network: the 2D square bond lattice ($p_c = 0.5$), the 2D triangular bond lattice ($p_c = 0.347$), and the 3D simple cubic bond lattice ($p_c = 0.2488$). The values of σ considered for the lognormal distribution ranged from 0.1 to 1.3, which equates to a coefficient-of-variation (CV) that ranged from 0.1 to 2.1. The computed ratios of the hydraulic and electrical conductivities were not dependent on the value of μ. For the power law distribution, the values of α ranged from −0.9 to 0.9. Also, two bounds were considered: $\delta_{max}/\delta_{min}$ equal to either 10^2 or 10^4. However, when $\delta_{max}/\delta_{min} = 10^4$, some larger α values produced networks with a very high degree of heterogeneity and the flow field could not be resolved numerically; those parameter combinations were discarded. The parameter combinations that were evaluated successfully for the power law distribution had CVs ranging from 0.6 to 2.3. Formulas for calculating CV, δ_g, and δ_c for the two distributions are given in the Appendix.

Skaggs [39] investigated the effects of boundary conditions and system size L on the computed mean conductivity of 3D networks (where where L is the number of nodes along one edge of the network). The mean network conductivity was shown to decrease towards an asymptotic value as the system size L was increased. The rate of approach to the asymptotic value depended on the boundary conditions (periodic vs. no flow) and the degree of network inhomogeneity. For highly disordered 3D networks with no-flow boundary conditions, Skaggs [39] found that $L \approx 18$ was typically sufficient to produce the asymptotic conductivity value (that is, further increasing L did not change the computed mean value), and ultimately used $L = 32$ to avoid finite-size effects. A similar analysis was done for the networks in the current paper and it was determined that 3D networks with $L = 32$ and 2D networks with $L = 128$ produced the asymptotic mean conductivity value; those are the system sizes used to compute the results reported below. It was verified that results were unchanged when $L = 64$ (3D) and $L = 256$ (2D).

3. Results

3.1. 3D networks

Fig. 1 compares the CPA predictions for 3D networks of cylindrical and slit-shaped pores (Eqs. (18) and (19), respectively) with the numerical data computed on cubic lattices with lognormal and

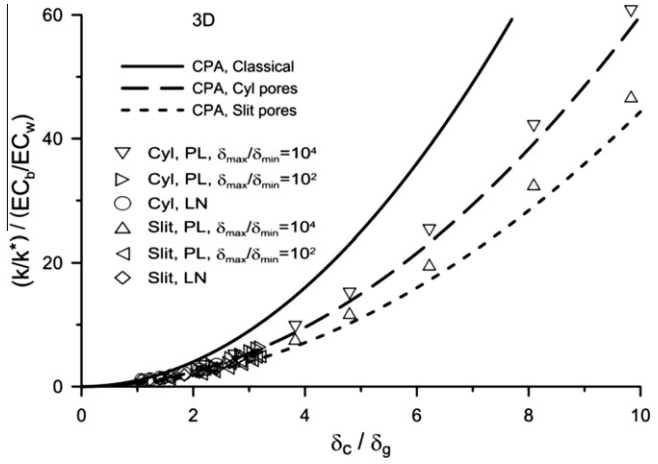

Fig. 1. Comparison of CPA predictions with numerical data computed for 3D cubic networks with cylindrical (Cyl) or slit-shaped (Slit) pores, and lognormally (LN) or power-law (PL) distributed pore-sizes.

power-law pore-size distributions. Also shown is the prediction of the classical CPA model, Eq. (20).

It is clear in Fig. 1 that the CPA model derived in the present work, Eqs. (18) and (19), is in better agreement with the numerical data than the classical CPA model. As predicted by Eqs. (18) and (19), the Monte Carlo data for cylindrical and slit-shaped pores diverge at larger values of the dimensionless critical pore size δ_c/δ_g. The new CPA model underestimates the data on average, whereas the classic CPA model overestimates the data. The error for the classic CPA was more severe for large values of δ_c/δ_g.

Fig. 2 presents the relative errors (difference between the prediction and the numerically computed value, divided by the numerically computed value) for the predictions shown in Fig. 1. Errors with respect to the individual data points in Fig. 1 are plotted as a function of the coefficient-of-variation (CV) of the pore-size distribution used in that simulation, which serves as a measure of the heterogeneity or disorder in the pore network. Fig. 2 shows that the accuracy of the new CPA model was better when heterogeneity was high. For relatively homogeneous pore distributions (CV = 0.1), the relative error was approximately −50% for the network with slit-shaped pores and −33% for the network with cylindrical pores. When heterogeneity was larger (CV > 0.75), predictions with the new CPA model were within ±20% of the data. The one exception was the network with lognormally distributed slit-shaped pores, where that level of accuracy was obtained only for CV > 1.

The results for the new CPA predictions are in contrast to those obtained with the classical CPA model (Fig. 2). The classical model overestimated the dimensionless conductivity ratio by an amount that became larger as pore heterogeneity was increased, with the error ranging from 12% in the most homogenous network to more than 100% in networks with higher heterogeneity. A similar trend in relative errors for the classical model can be observed by analyzing the CPA and numerical results presented in Fig. 5 of Friedman and Seaton [18].

3.2. 2D networks

Results for the square and triangular networks are presented in Fig. 3. Assuming $y = 0$, the classical CPA result and the CPA model derived herein are equivalent in 2D systems. Fig. 3 shows that the CPA prediction follows very well the general trend of the data obtained on 2D systems.

Fig. 4 gives the relative errors for the predictions shown in Fig. 3. The prediction error is within ±20% over the whole range

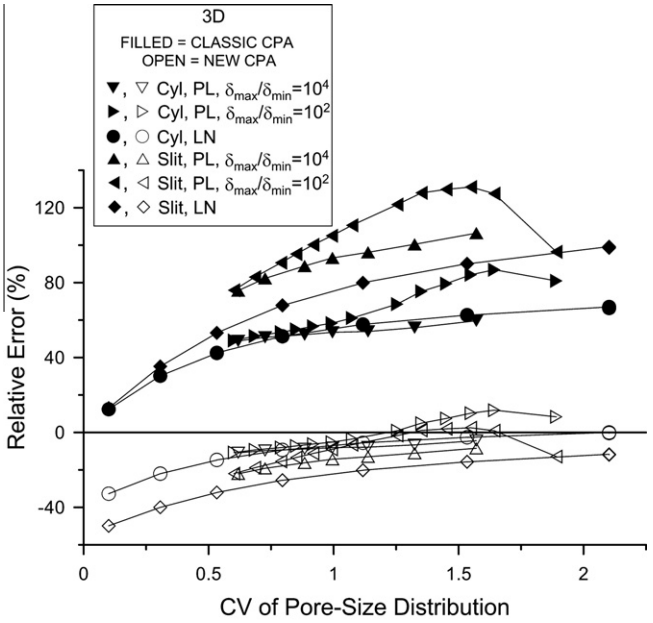

Fig. 2. Relative errors for the predictions shown in Fig. 1, plotted as a function of the coefficient-of-variation (CV) of the pore-size distribution.

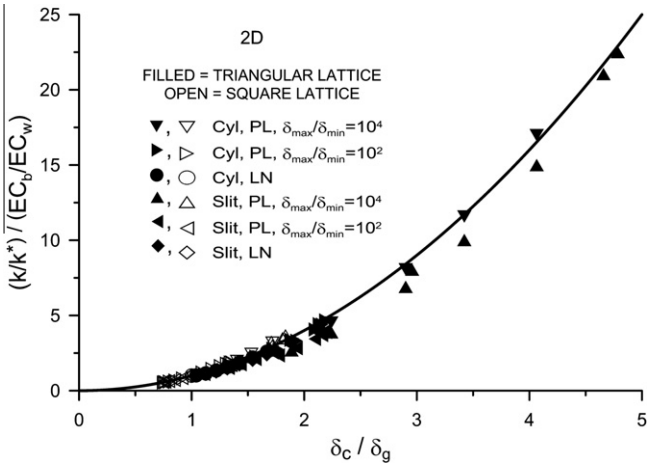

Fig. 3. Comparison of CPA predictions with numerical data computed for 2D square and triangular networks with cylindrical (Cyl) or slit-shaped (Slit) pores, and lognormally (LN) or power-law (PL) distributed pore-sizes.

of pore heterogeneity considered, expect in the case of slit-shaped pores on the triangular lattice with a power-law distribution, where that level of accuracy was obtained only at higher heterogeneity (CV > 1). Noteworthy in Fig. 4 is the fact that the error was zero for all cases with lognormally distributed pore-sizes on the square lattice. Overall, the errors were smaller for the square lattice than for the triangular lattice, a finding consistent with Friedman and Seaton's [18] observation that in 3D networks errors are smaller in networks with lower coordination numbers.

4. Discussion

A 2D network configured as a regular square bond lattice is a special case. Due to the self-dual properties of the square lattice, it can be shown that whenever the distribution of ln g is symmetric, the conductivity of the network is exactly equal to the geometric mean conductance [11]. And since $p_c = 0.5$ in the square lattice, it is also the case that g_c is equal to the geometric mean conduc-

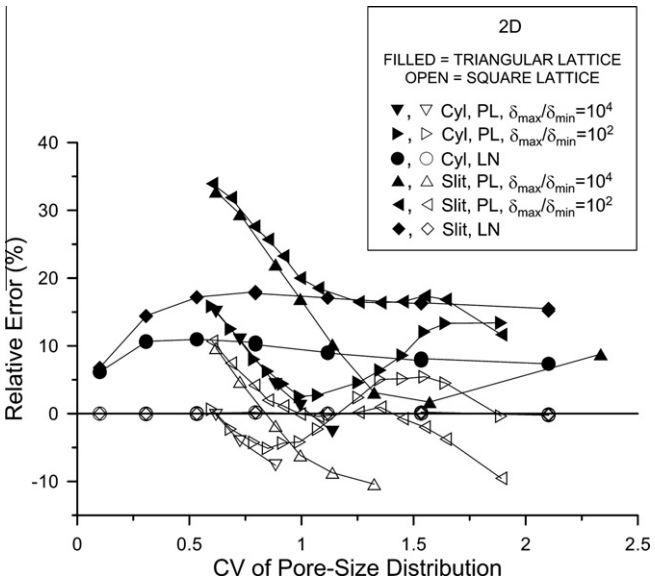

Fig. 4. Relative errors for the predictions shown in Fig. 3, plotted as a function of the coefficient-of-variation (CV) of the pore-size distribution.

tance when the distribution of ln g is symmetric. Thus for both log-uniform and lognormal distributions, the conductivity of the square lattice is equal to g_c regardless of width of the distribution, a result confirmed by our numerical computations (zero error for square lattices and lognormal distributions in Fig. 4). With $y = 0$, the CPA prediction agrees perfectly with this exact result.

The fact that the square lattice is a special case is not always recognized. Some previous numerical studies (e.g. [8,9]) used square lattices and log-symmetric distributions to assess the relevance of δ_c. As expected, those investigators found that δ_c was strongly related to the conductivity, although they apparently were not aware of the exact result for the conductivity. It is not possible to draw general conclusions about the applicability of CPA and other transport theories from such simulations. The importance of δ_c in this case is due to the particular properties of the lattice and the pore distribution, and exists regardless of whether flow is localized.

Investigating CPA mechanisms and predictions using 2D networks other than the square network is also problematic. In the CPA conception of transport in heterogeneous materials, the active transport pathways are typically envisioned as a macrostructure that exists on top of the underlying network. One model for the macrostructure is the "links-nodes-blobs" picture (e.g. [41]), such that transport occurs on connected chains of resistors that are called links. The macrostructure is comprised of an irregular network of such links. If the links are separated on average by a distance λ, and if the links have on average a conductance G, then the conductivity of the macrostructure is expected to be

$$\Sigma = \lambda^{2-d} G \tag{21}$$

where d (=2,3) is the spatial dimension. For $d = 2$, the conductivity in Eq. (21) does not depend directly with the path separation distance λ (indirectly, G will be affected by λ). Thus, 2D simulations alone are not appropriate for investigating CPA predictions about transport path separation or localization, and conclusions from such investigations should be weighted accordingly (e.g. [8–10,14,15]).

To understand the differences between the 3D CPA models (Eqs. (18) and (19) vs. Eq. (20)), recall that as heterogeneity in a network increases, the distance between transport pathways increases. For a given pore arrangement, the hydraulic conductance distribution will be broader (more heterogeneous) than the electrical conductance distribution owing the larger value of the exponent m in hydraulic conduction (Eqs. (5)–(9)). Consequently the separation of hydraulic pathways will be greater than that of electrical pathways. Similarly, for a given pore-size distribution, the cylindrical network produces a broader conductance distribution than the slit-shaped network due to the higher values of the exponents m. As was noted by Friedman and Seaton [18], Eq. (20) does not account for such differences in electrical and hydraulic conduction and in pore geometry. The leading terms in Eqs. (18) and (19) account for the differing path separations. Thus Eq. (20) becomes less accurate when heterogeneity is increased, whereas Eqs. (18) and (19) become more accurate.

Although Figs. 1 and 2 demonstrate that Eqs. (18) and (19) are an improvement over Eq. (20), that improvement comes at the expense of requiring knowledge of the local pore geometry (cylindrical or slit-shaped). An alternative comparison is obtained if instead of the two Eqs. (18) and (19), we use a single predictive equation that has the form of Eqs. (18) and (19), but with a leading numerical factor that is intermediate to those in Eqs. (18) and (19),

$$\frac{k/k^*}{EC_b/EC_w} = 2.5^{-y}(r_c/r_g)^2 \tag{22}$$

The accuracy of Eq. (22) was evaluated in terms of the relative prediction error, as done in Figs. 1 and 2. It was found that predictions with Eq. (22) were within ±25% of the numerical data when CV > 0.75, not dramatically different from the ±20% level of accuracy obtained with Eqs. (18) and (19), and still significantly better than the classical Eq. (20).

Thus far, all comparisons of pore network data and predictions have been based on data scaled by the pore geometry-dependent factor k^* and the geometric mean pore-size. While useful for model testing, one is more generally interested in predictive equations in the form of Eq. (4),

$$\frac{k}{EC_b/EC_w} = c\delta_c^2 \tag{23}$$

where c is a numerical constant. Putting Eqs. (18) and (19) in the form of Eq. (23), we obtain $c \equiv c_{CY} = 2^{-y}/32 \approx 1/53$ for cylindrical pores and $c \equiv c_{SL} = 3^{-y}/12 \approx 1/27$ for slit-shaped pores. It is interesting to consider how Eq. (23) with these constant values compares with an arbitrary model of the form $c\delta_c^p$, where c and p are optimized to minimize the squared deviations from the numerical data. Fig. 5 presents Eq. (23) along with the results of the fitting for cylindrical and slit-shaped pores. The results in Fig. 5 indicate that for networks having pore-size distributions with CV > 0.75, the constants obtained in the CPA model are nearly optimal in terms of minimizing the squared prediction error across the range of considered network configurations.

With respect to applications to real porous media, it was noted above that Katz and Thompson [26,27] (hereafter KT) used CPA to derive the value $c \equiv c_{KT} \approx 1/226$. KT estimated that this value was accurate to within a factor of 2 based on an evaluation of permeability, electrical conductivity, and mercury intrusion data for various rock samples having permeabilities that spanned approximately 6 decades. However, some details of KT's theoretical derivation have been criticized [5,32], leaving open the question of a satisfactory theoretical calculation that produces a numerical constant which agrees with the KT data. KT's calculation was for a network of cylindrical pores in which the diameters were equal to their lengths. Banavar and Johnson [5] and Le Doussal [32] did CPA calculations for the same network and found c to be approximately 1/130 and 1/85, respectively, the former being within the confidence bounds of KT's data. Still, these calculations may also be questioned, as it has been noted that a network of cylindrical pores with lengths equal to the diameters may not be physically realizable or otherwise realistic (e.g. [18,21]). A common

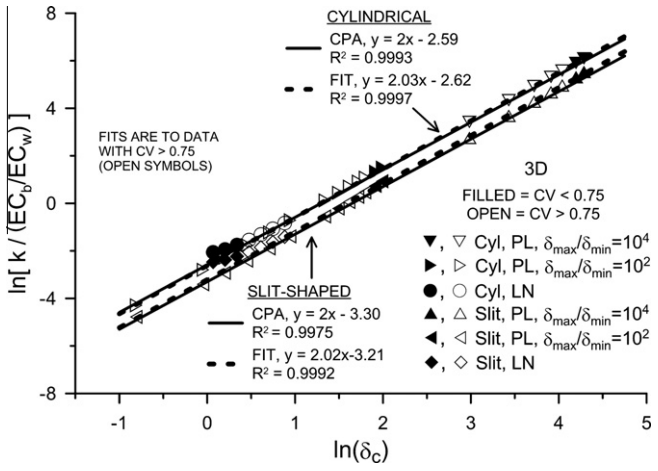

Fig. 5. Comparison of the CPA model with the equation $c\delta_c^p$, where c and p have been optimized to minimize the squared deviations from the data. Numerical data are form 3D cubic networks with cylindrical (Cyl) or slit-shaped (Slit) pores, and lognormally (LN) or power-law (PL) distributed pore-sizes.

alternative is a network in which the pores have a fixed, uniform length, such as the networks considered in the current study. For such a network of cylindrical pores, Banavar and Johnson [5] and Le Doussal [32] obtained 1/87 and 1/59, respectively, which are comparable with the value obtained here, $c_{CY} = 1/53$ (the difference between c_{CY} and the value from [32] is due only to differing values of y being used in the calculations). These values are 2.6–4.3 times larger than c_{KT} and outside the confidence bounds given for the KT data. Le Doussal [32] has shown that adding additional disorder or randomness to networks of cylindrical pores, such as in the pore length, may lead to coefficients in better agreement with the experimental data.

Not previously considered is a comparison of the KT data with calculations for a regular network of slit-shaped pores. This comparison requires a modification of the KT data because KT's measurement of δ_c was based on the Washburn equation for cylindrical pores. Reconsidering the KT data in terms of slit-shaped pores leads to a constant that is 4 times larger, $c \approx 1/57$. The value estimated in the present work, $c_{SL} = 1/27$, is about a factor of 2 larger than this value, and at the edge of the confidence bounds for the KT data. Thus, coefficients calculated for a regular network of slit-shaped pores are in better agreement with experimental data than those calculated for a regular network of cylindrical pores.

5. Summary and conclusions

Several past applications of critical path analysis (CPA) to pore network models have produced results that appeared to be in contradiction to long-standing notions about CPA, or otherwise raised questions about the applicability of CPA to porous media. To clarify the performance of CPA on pore network models, numerical computations of the permeability and electrical conductivity of 2D and 3D pore networks were compared with CPA predictions. A new CPA model for the relationship between the permeability and electrical conductivity was found to be in good agreement with the numerical data, and to be a significant improvement over a classical CPA model. In sufficiently disordered 3D networks, the new CPA model was within ±20% of the true value, and was nearly optimal in terms of minimizing the squared prediction errors across differing network configurations. The agreement of CPA predictions with 2D network computations was similarly good, although it was observed that 2D networks are in general not well-suited for evaluating CPA. Numerical transport coefficients derived for 3D networks of slit-shaped pores were found to be in better agreement with experimental data from rock samples than was coefficients derived for networks of cylindrical pores.

Appendix

The formulas in this appendix were used to calculate the coefficient-of-variation (CV) for the pore-size distributions, the geometric mean pore-size (δ_g), and the critical pore-size (δ_c). The latter is defined by

$$p_c = \int_{\delta_c}^{\infty} f_\delta(\delta)d\delta \tag{A1}$$

where f_δ is the pore-size probability density function and p_c is the percolation threshold for the network. The percolation thresholds for the lattices used in this work are $p_c = 0.5$ for the square lattice, $p_c = 0.347$ for the triangular lattice, and $p_c = 0.2488$ for the cubic lattice [41].

For the power law distribution (Eq. (10)), the following formulas apply ($\alpha \neq 0, 1, 2$):

$$\mathrm{CV} = S/M \tag{A2}$$

$$M = \frac{\alpha\left(\delta_{\min}\delta_{\max}^{\alpha} - \delta_{\min}^{\alpha}\delta_{\max}\right)}{(\alpha-1)\left(\delta_{\max}^{\alpha} - \delta_{\min}^{\alpha}\right)} \tag{A3}$$

$$S^2 = \frac{\delta_{\min}^2\delta_{\max}^{2\alpha} + \delta_{\min}^{2\alpha}\delta_{\max}^2 - (\alpha-1)^2(\delta_{\min}^{\alpha}\delta_{\max}^{\alpha+2} + \delta_{\min}^{\alpha+2}\delta_{\max}^{\alpha}) + 2\alpha(\alpha-2)\delta_{\min}^{\alpha+1}\delta_{\max}^{\alpha+1}}{\alpha^{-1}(\alpha-1)^2(\alpha-2)\left(\delta_{\max}^{\alpha} - \delta_{\min}^{\alpha}\right)^2} \tag{A4}$$

$$\delta_c = \left[p_c\delta_{\min}^{-\alpha} + (1-p_c)\delta_{\max}^{-\alpha}\right]^{-1/\alpha} \tag{A5}$$

$$\delta_g = \exp(1/\alpha)\delta_{\min}^{\gamma}\delta_{\max}^{1-\gamma} \tag{A6}$$

where $\gamma \equiv \delta_{\max}^{\alpha}/(\delta_{\max}^{\alpha} - \delta_{\min}^{\alpha})$.

For the lognormal distribution (Eq. (12)), we have

$$\mathrm{CV} = \left[\exp(\sigma^2) - 1\right]^{1/2} \tag{A7}$$

$$\delta_c = \exp\left[2^{1/2}\sigma\,\mathrm{erfc}^{-1}(2p_c) + \mu\right] \tag{A8}$$

$$\delta_g = \exp[\mu] \tag{A9}$$

where $\mathrm{erfc}^{-1}(\cdot)$ is the inverse complementary error function.

References

[1] Adler PM. Porous media: geometry and transports. Boston: Butterworth-Heinemann; 1992.
[2] Agrawal DL, Cook NGW, Myer LR. The effect of percolating structures on the petrophysical properties of Berea sandstone. In: Proceedings of the 32nd US Rock Mechanical Symposium; 1991. p. 345–54.
[3] Ambegaokar V, Halperin BI, Langer JS. Hopping conductivity in disordered systems. Phys Rev B 1971;4:2612–20.
[4] Angulo RF, Medina E. Critical path analysis of conductance fluid invasion and rupture. Physica A 1996;232:21–6.
[5] Banavar JR, Johnson DL. Characteristic pore sizes and transport in porous media. Phys Rev B 1987;35:7283–6.
[6] Berkowitz B, Balberg I. Percolation theory and its application to groundwater hydrology. Water Resour Res 1993;29:775–94.
[7] Berkowitz B, Ewing RP. Percolation theory and network modeling applications in soil physics. Surv Geophys 1998;19:23–72.
[8] Bernabé Y. The transport properties of networks of cracks and pores. J Geophys Res 1995;100:4231–41.
[9] Bernabé Y, Bruderer C. Effect of the variance of pore size distribution on the transport properties of heterogeneous networks. J Geophys Res 1998;103:513–25.
[10] Bernabé Y, Revil A. Pore scale heterogeneity, energy-dissipation and the transport-properties of rocks. Geophys Res Lett 1995;22:1529–32.
[11] Bernasconi J, Schneider WR, Wiesmann HJ. Some rigorous results for random planar conductance networks. Phys Rev B 1977;16:5250–5.
[12] Bottger H, Bryksin VV. Hopping conduction in solids. Derrfield Beach, FL: VCH; 1985.
[13] Das DB, Hassanizadeh SM, editors. Upscaling multiphase flow in porous media: from pore to core and beyond. The Netherlands: Springer; 2005.

[14] David C, Gueguen Y, Pampoukis G. Effective medium theory and network theory applied to the transport properties of rock. J Geophys Res 1990;95:6993–7005.
[15] David C. Geometry of flow paths for fluid transport in rocks. J Geophys Res 1993;98:12267–78.
[16] Dullien FAL. Porous media: fluid transport and pore structure. 2nd ed. San Diego, CA: Academic Press; 1992.
[17] Feng S, Halperin BI, Sen PN. Transport properties of continuum systems near the percolation threshold. Phys Rev B 1987;35:197–214.
[18] Friedman SP, Seaton NA. Critical path analysis of the relationship between permeability and electrical conductivity of three-dimensional pore networks. Water Resour Res 1998;34:1703–10.
[19] Halperin BI. Remarks on percolation and transport in networks with a wide range of bond strengths. Physica D 1989;38:179–83.
[20] Hunt AG. Applications of percolation theory to porous media with distributed local conductances. Adv Water Resour 2001;24:279–307.
[21] Hunt A, Ewing R. Percolation theory for flow in porous media. Lecture notes in physics, vol. 771. New York: Springer; 2009.
[22] Hunt AG, Gee GW. Application of critical path analysis to fractal porous media: comparison with examples from the Hanford site. Adv Water Resour 2002;25:129–46.
[23] Hunt AG, Gee GW. Water-retention of fractal soil models using continuum percolation theory: tests of Hanford site soils. Vadose Zone J 2002;1:252–60.
[24] Hunt AG, Gee GW. Wet-end deviations from scaling of the water retention characteristics of fractal porous media. Vadose Zone J 2003;2:759–65.
[25] Hunt AG, Idriss B. Percolation-based effective conductivity calculations for bimodal distributions of local conductances. Philos Mag 2009;89:1–21.
[26] Katz AJ, Thompson AH. Quantitative prediction of permeability in porous rock. Phys Rev B 1986;34:8179–81.
[27] Katz AJ, Thompson AH. Prediction of rock electrical conductivity from mercury injection measurements. J Geophys Res 1987;92:599–607.
[28] Kolek A, Snarskiĭ AA, Morozovskiĭ AE. Structure of the percolation cluster and excess $1/f$ noise in systems with an exponentially broad spectrum of resistances. J Exp Theoret Phys 1995;81:490–5.
[29] Kosugi K. Three-parameter lognormal distribution model for soil water retention. Water Resour Res 1994;30:891–901.
[30] Kurkijärvi J. Conductivity in random systems. II. Finite-size-system percolation. Phys Rev B 1974;39:770–4.
[31] Le Doussal P. Percolation like exponent for the conductivity of highly disordered resistor networks. Phys Rev B 1989;39:881–4.
[32] Le Doussal P. Permeability versus conductivity for porous media with wide distribution of pore sizes. Phys Rev B 1989;39:4816–9.
[33] Liang Z, Ioannidis MA, Chatzis I. Permeability and electrical conductivity of porous media from 3D stochastic replicas of the microstructure. Chem Eng Sci 2000;55:5247–62.
[34] Lukasiewicz SJ, Reed JS. Specific permeability of porous compacts as described by a capillary model. J Am Ceram Soc 1988;71:1008–14.
[35] Moldrup P, Olesen T, Komatsu T, Schjønning P, Rolston DE. Tortuosity, diffusivity, and permeability in the soil liquid and gaseous phases. Soil Sci Soc Am J 2001;65:613–23.
[36] Purvance DT, Andricevic R. On the electrical–hydrualic conductivity correlation in aquifers. Water Resour Res 2000;36:2905–13.
[37] Reed JS. Liquid permeability of packed particles: why perpetuate the Carmen–Kozeny model? J Am Ceram Soc 1993;76:547–8.
[38] Seager CH, Pike GE. Percolation and conductivity: a computer study. II. Phys Rev B 1974;10:1435–46.
[39] Skaggs TH. Effects of finite system-size and finite inhomogeneity on the conductivity of broadly distributed resistor networks. Physica B 2003;338:266–9.
[40] Slater L, Lesmes DP. Electrical–hydraulic relationships observed for unconsolidated sediments. Water Resour Res 2002;38. doi:10.1029/2001WR001075.
[41] Stauffer D, Aharony A. Introduction to Percolation Theory. Revised 2nd ed. Philadelphia: Taylor and Francis; 1994.
[42] Torquato S. Random heterogeneous materials. New York: Springer-Verlag; 2002.
[43] Tyč S, Halperin BI. Random resistor network with an exponentially wide distribution of bond conductances. Phys Rev B 1989;38:877–80.
[44] Wildenschild D, Roberts JJ, Carlberg ED. On the relationship between microstructure and electrical and hydraulic properties of sand–clay mixtures. Geophys Res Lett 2000;27:3085–8.